Coupling of Wideband Radiated IEMI to Cables above Ground

Tao Liang, Giordano Spadacini, *Senior Member, IEEE,* Flavia Grassi, *Senior Member, IEEE*, and Sergio A. Pignari, *Fellow, IEEE*

***Abstract*—In this work, transmission-line (TL) theory is applied to formulate a worst-case analysis for the assessment of wideband intentional electromagnetic interference (IEMI) radiated onto a cable harness (with terminal units) above ground. Given the bandwidth and the energy density of the high-power electromagnetic (HPEM) pulse impinging on the cable, the pulse spectrum maximizing the peak value of the common-mode (CM) voltage waveform induced at a cable end is obtained. Unlike in a full-wave solution to the problem, the proposed TL model allows for a) deriving closed-form expressions in the special case of a cable terminated in a matched load at the opposite end; b) computationally efficient evaluation of the spectrum for any other loading conditions. The obtained results clearly unveil the impact of the system parameters (cable length, height, terminal loads and pulse bandwidth) on the statistics of the worst-case voltage peak for random direction of incidence and polarization.**

***Index Terms*—High-power electromagnetic (HPEM) pulse, intentional electromagnetic interference (IEMI), statistical electromagnetic compatibility (EMC) models.**

I. Introduction

In a recent paper [1], a combined worst-case/statistical approach was proposed for modeling coupling effects of wideband intentional electromagnetic interference (IEMI) radiated onto systems composed of linear metallic/dielectric materials. Given the bandwidth and the energy density of a high-power electromagnetic (HPEM) pulse, impinging on the victim system in the form of a linearly polarized plane-wave field, the problem consists in finding the worst-case spectrum, and the associated pulse, leading to the maximum peak value of the voltage induced across an electric port of interest. Consequently, there is no need to specify the waveform/spectrum belonging to the wide and general definition of sub-hyperband or hyperband HPEM pulse [2]. As a matter of fact, experimental data demonstrate that wideband spectra may be quite different and related to the specific technology implemented in the radiating disruptor [3, Fig. 1], [4, Figs. 1-3], [5, Fig. 2-3], [6, Fig. 5]. The worst-case solution proposed in [1] leaves such spectra out of consideration and finds the HPEM pulse which is optimally matched to the receiving characteristics of the victim system (in the specified bandwidth), thus providing a conservative assessment of expected disturbances.

Furthermore, since the worst-case solution depends on the direction of incidence and polarization angle of the plane wave, which are unknown in a real IEMI-attack scenario, a statistical approach can be used to model such quantities as random variables (RVs) and to estimate the cumulative distribution function (cdf) of the worst-case peak voltage through a Monte Carlo analysis. In [1], repeated-run simulations were conveniently accelerated by the assumption of linearity and the use of the Lorentz reciprocity theorem. Namely, the victim structure is preliminarily treated as an unintentional transmitting antenna and solved (by a single full-wave simulation, carried out through any suitable numerical code) for its radiation pattern and input impedance. Then, by invoking the reciprocity theorem, the aforementioned quantities are used to evaluate the voltage induced by an impinging HPEM plane wave field, for any possible direction of incidence and polarization.

The approach described above is quite general, since it is based on full-wave simulation, which may cope with any complex 3D system. However, in several cases, the victim structures of interest involve long cable interconnects [6], [7]. Actually, the external cables (especially if unshielded) can be considered one of the main contributors to the overall coupling of the HPEM field. The dominant effect in the coupling mechanism is the induction of common-mode (CM) currents and voltages propagating along the wiring harness and entering the ports of equipment [7]. Finally, the terminal imbalance of differential interfaces determines the conversion of CM into differential mode.

In terms of computational efficiency, it is well known that coupling of radiated fields with cable harness is optimally predicted by transmission-line (TL) models rather than by full-wave methods [8]. Indeed, provided that the basic assumption of transverse-electromagnetic (TEM) mode is met, TL models allow avoiding fine three-dimensional meshing of the region of space along and around electrically-long cables [9]. Consequently, the full-wave modeling approach presented in [1] is not best suited for the analysis of a wiring harness.

To overcome this drawback, this paper exploits TL theory to formulate and solve the optimization problem leading to the worst-case HPEM pulse for a bundle with terminal units, running above a ground plane. The obtained solution allows for closed-form expressions of the worst-case CM voltage peak induced across the bundle loads in the specific case of matched terminations. In the case of arbitrary loading conditions, the

Manuscript received June 19, 2018; revised Sept. 21, 2018; accepted Oct. 15, 2018.

The authors are with Dipartimento di Elettronica, Informazione e Bioingegneria (DEIB), Politecnico di Milano, Milan, 20133 Italy. (email: {tao.liang, giordano.spadacini, flavia.grassi, sergio. pignari}@polimi.it)

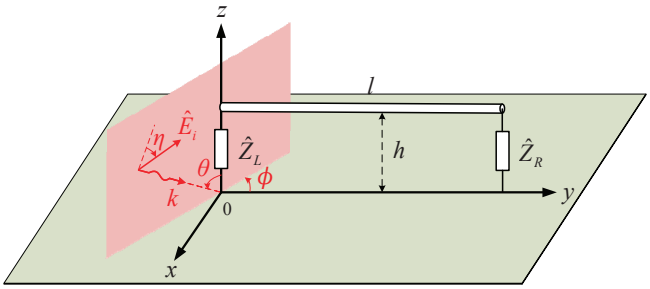

Fig. 1. TL illuminated by a linearly polarized uniform plane wave.

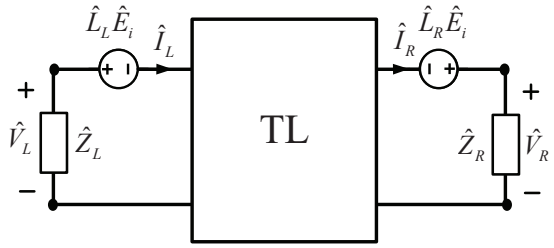

Fig. 2. Equivalent circuit representation of a TL illuminated by an external field.

solution involves numerical computation of some integrals that can be carried out with limited effort. From the interpretation of the closed-form expressions and/or numerical simulations, a number of general properties are inferred, which explain the role played by the geometrical and electrical parameters of the system configuration under analysis (i.e., cable length and height, terminal impedances, and pulse bandwidth).

The paper is organized as follows. Section II presents the structure under analysis, the TL model and the spectrum/waveform of the worst-case HPEM pulse and the induced voltage. Results are compared with the full-wave formulation in [1] and applicability limits are stated. In Section III, the impact of system parameters on the worst-case CM voltage peak induced at the cable terminals is investigated through analytical derivations and numerical simulations. The inferred properties are further corroborated by Monte Carlo simulations presented in Section IV and aimed at evaluating the cdf of the worst-case voltage peak in case of random direction of incidence and polarization. Finally, Section V draws concluding remarks.

II. Worst-Case Radiated HPEM Pulse for an Unshielded Cable Running Above Ground

A. Structure Under Analysis and TL Model

An unshielded cable harness running above a metallic ground is excited by an HPEM plane-wave pulse, described by an incident electric field $E_i(t)$ with finite energy density W (in J/m^2), whose frequency-domain spectrum $\hat{E}_i$ is bandlimited in an angular-frequency interval $[\omega_1, \omega_2]$, that is, a frequency interval $[f_1, f_2]$. In Fig. 1, angles θ, ϕ define the direction of incidence, whereas angle η describes the polarization.

The following analysis focuses on the dominant CM coupling mechanism, with the twofold objective of generalization (e.g., irrespective of the harness cross-section) and simplification (e.g., derivation of closed-form solutions). In line with this aim, the harness is represented by an equivalent CM model, composed of a bare wire of length l, radius r_w, running at height h above ground, with CM impedances $\hat{Z}_L$, $\hat{Z}_R$ connected to ground at the left and right end, respectively. It is anyway worth noting that any specific configuration of the wiring harness could be accounted for by a straightforward multiconductor extension of the proposed model [8].

Without loss of generality, the port of interest for the evaluation of interference is the left one, and the target variable is the CM voltage waveform $V_L(t)$ induced across $\hat{Z}_L$. Under the assumption $h \ll c_0/f_2$ (where $c_0 = 1/\sqrt{\mu_0\varepsilon_0}$ is the speed of light, μ_0 and ε_0 are the vacuum permeability and permittivity, respectively), the scattered CM field has a dominant TEM configuration, which can be modeled by TL theory [8]. Since the involved frequency-domain formulations are well-known [9], just the final solution is here reported in the most suitable form.

For the computation of terminal voltages and currents, the TL can be represented by the equivalent circuit model in Fig. 2, where the central two-port network is described by the chain-parameter matrix $\hat{\mathbf{\Phi}}$:

$$\hat{\mathbf{\Phi}} = \begin{bmatrix} \hat{\Phi}_{11} & \hat{\Phi}_{12} \\ \hat{\Phi}_{21} & \hat{\Phi}_{22} \end{bmatrix} = \begin{bmatrix} \cos(\beta l) & -jZ_C \sin(\beta l) \\ -jZ_C^{-1} \sin(\beta l) & \cos(\beta l) \end{bmatrix} \quad (1)$$

where j is the imaginary unit, $Z_C = \sqrt{\mu_0/\varepsilon_0}\ln(2h/r_w)/2\pi$ is the line characteristic impedance, and $\beta = 2\pi f/c_0$ is the phase constant. The left and right voltage sources $\hat{L}_L\hat{E}_i$, $\hat{L}_R\hat{E}_i$ are linearly dependent on $\hat{E}_i$, and the involved transfer functions are expressed by:

$$\hat{L}_L = -2h\left(\frac{je^{-j\beta l \sin\theta\cos\phi} - j\cos(\beta l)}{\sin(\beta l)}F + H\right) \quad (2)$$

$$\hat{L}_R = e^{-j\beta l \sin\theta\cos\psi}\hat{L}_L^*$$

$$F = \frac{\cos\theta(\cos\theta\cos\phi\cos\eta + \sin\phi\sin\eta)}{1-\sin^2\theta\cos^2\phi} \quad (3)$$

$$H = -F\sin\theta\cos\phi + \sin\theta\cos\eta$$

where the asterisks * denotes complex conjugation. By solving the circuit model in Fig. 2, the induced voltage can be cast as

$$\hat{V}_L = \hat{L}(\omega)\hat{E}_i \quad (4)$$

where a frequency-dependent *coupling length*

$$\hat{L}(\omega) = \hat{Z}_L \frac{(\hat{\Phi}_{11} - \hat{Z}_R\hat{\Phi}_{21})\hat{L}_L - \hat{L}_R}{\hat{Z}_R\hat{\Phi}_{22} - \hat{Z}_R\hat{\Phi}_{21}\hat{Z}_L - \hat{\Phi}_{12} + \hat{\Phi}_{11}\hat{Z}_L} \quad (5)$$

is analytically defined to replace the same full-wave quantity introduced in [1].

B. Worst-case Spectra and Waveforms

By applying the inverse Fourier transform (IFT) to (4), the time-domain waveform of the induced voltage is obtained as

$$V_L(t) = \frac{1}{2\pi}\int_{-\infty}^{+\infty} \hat{L}(\omega)\hat{E}_i(\omega)e^{j\omega t}d\omega \tag{6}$$

where $\hat{E}_i(-\omega) = \hat{E}_i(\omega)^*$. It is of interest to find the worst-case electric-field spectrum which maximizes the peak of the induced voltage at an arbitrary time instant t_0, i.e.,

$$V_{LP} = V_L(t_0) = \max\{V_L(t)\} \tag{7}$$

under the total-energy constraint

$$W = \frac{1}{2\pi Z_0}\int_{-\infty}^{+\infty} \left|\hat{E}_i(\omega)\right|^2 d\omega \tag{8}$$

where $Z_0 = \sqrt{\mu_0/\varepsilon_0}$ is the wave impedance. This constrained-optimization problem is formally the same as the one solved in [1], hence the relevant conclusions are still valid, provided that the coupling length is now expressed by (5). According to the derivations presented in [1], the worst-case HPEM spectrum results to be

$$\hat{E}_i(\omega) = \sqrt{\frac{Z_0\pi W}{\int_{\omega_1}^{\omega_2}\left|\hat{L}(\omega)\right|^2 d\omega}}\hat{L}(\omega)^* e^{-j\omega t_0} \tag{9}$$

which leads to the worst-case CM voltage peak

$$V_{LP} = \sqrt{\frac{Z_0 W}{\pi}\int_{\omega_1}^{\omega_2}\left|\hat{L}(\omega)\right|^2 d\omega} \tag{10}$$

on condition the integrals in (9) and (10) are finite, that is, $\hat{L}(\omega)$ is a square-integrable function. This condition is generally verified except for very special cases of limited interest, where singularities of the coupling length are originated by the ideality of the model. For instance, since (5) is derived from a lossless TL model, $\hat{L}(\omega)$ exhibits singularities in case of ideal open-circuits connected at both line terminals.

According to the worst-case solution (9), the field spectrum is optimally matched, in energetic terms, with the receiving properties of the victim equipment, described by the coupling length, in the frequency band of interest and for a specified incidence and polarization of the electromagnetic field. In fact, the obtained expression obeys a maximum power transfer condition, where the magnitude of the electric field spectrum is proportional to the magnitude of the coupling length, whereas phase angles are complex conjugated (except for an arbitrary shift ωt_0 which sets the desired instant t_0).

C. Validation and Limitation

For a structure with l =1 m, r_w=1 mm, h=1 cm, $\hat{Z}_L = 180\,\Omega$, $\hat{Z}_R = 10\,\Omega$, θ=60°, ϕ=120°, η=135°, excited by a hyperband HPEM pulse carrying an energy density W=1 mJ/m^2 in the band [300 MHz, 3 GHz], the coupling length is plotted in Fig. 3 as obtained by the proposed TL model (5), and by the reciprocity-based approach [1] implemented through a full-wave finite-integration-technique (FIT) solver [10].

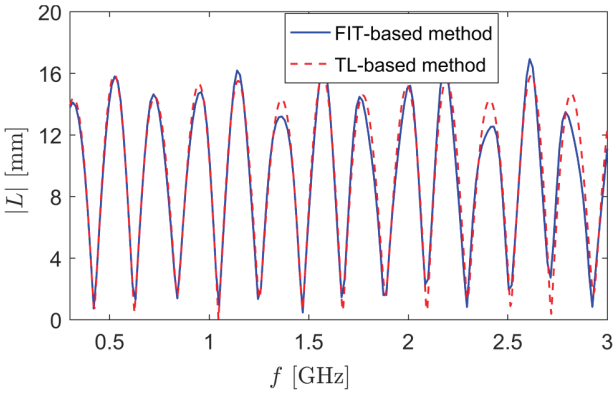

Fig. 3. Comparison of the coupling length predicted by full-wave simulation and TL model. Data: l =1 m, r_w=1 mm, h=1 cm, $\hat{Z}_L = 180\,\Omega$, $\hat{Z}_R = 10\,\Omega$, θ=60°, ϕ=120°, η=135°.

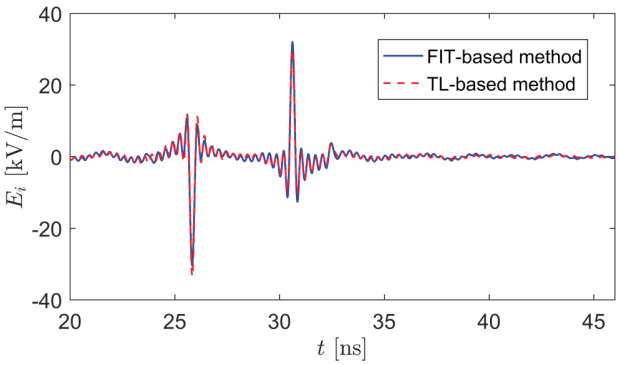

Fig. 4. Comparison of the worst-case waveform of the impinging electric field predicted by the FIT-based method and the proposed TL-based method. Data: l =1 m, r_w=1 mm, h=1 cm, $\hat{Z}_L = 180\,\Omega$, $\hat{Z}_R = 10\,\Omega$, θ=60°, ϕ=120°, η=135°.

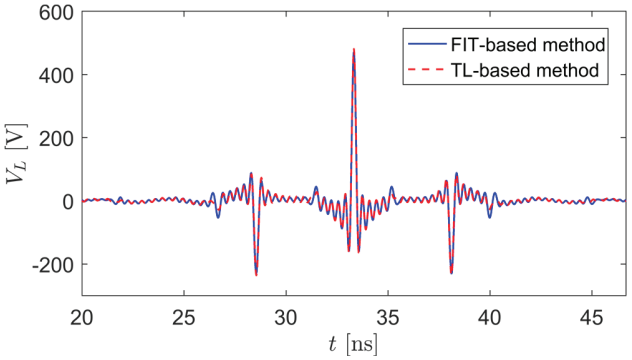

Fig. 5. Comparison of the worst-case induced voltage at the EUT ports predicted by the FIT-based method and the proposed TL-based method. Data: l =1 m, r_w=1 mm, h=1 cm, $\hat{Z}_L = 180\,\Omega$, $\hat{Z}_R = 10\,\Omega$, θ=60°, ϕ=120°, η=135°.

The IFT of (9) with t_0 = 33 ns leads to the worst-case electric-field $E_i(t)$ in Fig. 4, and to the CM voltage $V_L(t)$ in Fig. 5. The time axis is limited in the window [20, 46.7] ns just for optimal readability. These results confirm that the TL formulation provides good prediction of the worst-case waveforms. Minor errors are mainly localized at peaks, e.g.: -33.4 kV/m (TL), -

30.6 kV/m (FIT) in Fig. 4. The worst-case induced voltage peaks are V_{LP}= 481 V (TL) and V_{LP}= 471 V (FIT) in Fig. 5.

These different outputs of the proposed TL method and the full-wave method [1] are in fair agreement. Discrepancies can be ascribed to high-order propagation modes occurring in the high-frequency range, not accounted for by TL theory. In strict terms, the TL method should be accurate for a line height h less than 1/10 of the wavelength, that is, for frequencies $f<c_0/(10h)$ so that the TEM propagation mode is dominant. Since a hyperband spectrum is of interest, which has an integral effect on time-domain results, errors for high-frequency peak/notches (see Fig. 3) can be accepted if most of the other frequency components are correctly evaluated. As a rule of thumb, the validity condition for the TL approach can be relaxed to no more than $f_2<c_0/(5h)$ with reference to the maximum frequency. Otherwise, the full-wave approach presented in [1] is recommended.

The lack of accuracy is well compensated by computational efficiency. Namely, the TL model takes less than one second on a personal computer (Intel i7-6700, RAM 16 GB), whereas the full-wave approach requires about 30 minutes [11].

III. Impact of Line Length, Height, CM Impedances and Pulse Bandwidth

A. Special Case of Matched Load at the Opposite End

A simple closed-form expression of the worst-case voltage peak (10) can be obtained under the simplifying assumption of a resistive impedance $\hat{Z}_L = R_L$ connected at the port of interest, and a resistive matched load $\hat{Z}_R = R_R = Z_C$ connected at the opposite TL terminal. Accordingly, the coupling length (5) can be recast as

$$\hat{L}(\omega) = -\frac{4jR_L hG}{R_L + Z_C}\sin\left(\frac{\beta l}{2}\left(1+\sin\theta\cos\phi\right)\right)e^{-j\frac{\beta l}{2}(1+\sin\theta\cos\phi)} \qquad (11)$$

where G is determined by incidence and polarization angles

$$G = \cos\eta\frac{\cos\phi+\sin\theta}{1+\sin\theta\cos\phi} + \sin\eta\frac{\cos\theta\sin\phi}{1+\sin\theta\cos\phi} \qquad (12)$$

for $1+\sin\theta\cos\phi \neq 0$, otherwise $\hat{L}(\omega)=0$. The substitution of (11) in (10) leads to

$$V_{LP} = 4h|G|\frac{R_L}{R_L+Z_C}\sqrt{\frac{Z_0 W}{\pi}}\times \sqrt{\frac{\omega_2-\omega_1}{2} - \frac{\sin\left(\frac{\omega_2 l}{c_0}\left(1+\sin\theta\cos\phi\right)\right)-\sin\left(\frac{\omega_1 l}{c_0}\left(1+\sin\theta\cos\phi\right)\right)}{\frac{2l}{c_0}\left(1+\sin\theta\cos\phi\right)}} \qquad (13)$$

A plot of V_{LP} versus l is presented in Fig. 6 (for data in Section II.C except for R_R =Z_C=180 Ω). It can be observed that *V_{LP} converges to an asymptote V_∞ for long lines*. Indeed, since

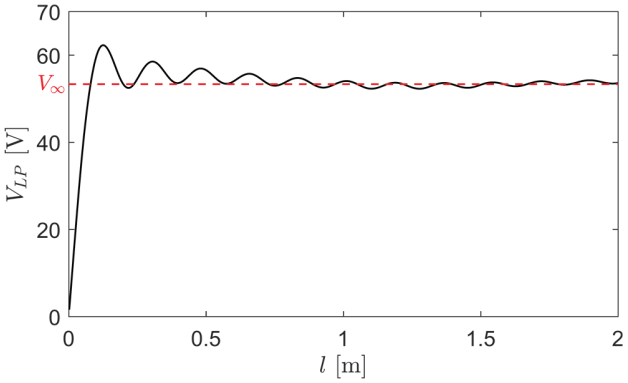

Fig. 6. Peak voltage V_{LP} vs harness length l for $R_R = 180\ \Omega$ (matched load). Other data: r_w=1 mm, h=1 cm, R_L=180 Ω, θ=60°, ϕ=120°, η=135°.

the radicand in (13) oscillates around $(\omega_2-\omega_1)/2$ and the difference of two sines is bounded by the interval [-2, 2], a convergence criterion can be stated as

$$\frac{\omega_2-\omega_1}{2} \gg \frac{2}{\frac{2l}{c_0}\left(1+\sin\theta\cos\phi\right)} \qquad (14)$$

which leads to the condition

$$l >> l_s = \frac{c_0}{\pi B\left(1+\sin\theta\cos\phi\right)} \qquad (15)$$

where $B = f_2 - f_1$ is the pulse bandwidth. For short lines ($l < l_s$) the worst-case voltage peak increases almost linearly with the line length, whereas for a long harness it can be approximated by the following asymptote (the error is less than 5% for $l > 10l_s$)

$$V_\infty = 4h|G|\frac{R_L}{R_L+Z_C}\sqrt{Z_0 WB} \qquad (16)$$

which is simply *proportional to the square root of the bandwidth*. With reference to Fig. 6, $l_s = 0.06$ m, $V_\infty = 53.3$ V.

Both in (13) and (16) the impact of other system parameters can be easily identified. Particularly, the worst-case voltage peak results to be almost *proportional to the line height* (the multiplicative term h is dominant over the logarithmic dependence of Z_C on h). Additionally, the resistance R_L connected to the port of interest simply acts through a *voltage divider* $R_L/(R_L+Z_C)$.

As far as the dependence on wave angles is concerned, the extreme value of (13) and (16) is reached for $|G|$=1, which occurs for infinite combinations of incidence and polarization angles, according to (12). Some noteworthy cases are a) side-fire (θ=90°, ϕ=0°) or broadside incidence (θ=ϕ=90°) with vertical electric field (η=0°); b) top incidence (θ=0°, ϕ=0°) with horizontal electric field tangent to the wire (η=0°).

B. General Loading Conditions

For an arbitrary load R_R connected at the opposite line end, the worst-case voltage peak (10) cannot be expressed in closed-form. Nevertheless, the role of system parameters can be investigated by numerical simulations, using a quadrature method to evaluate integrals over the bandwidth. Without loss

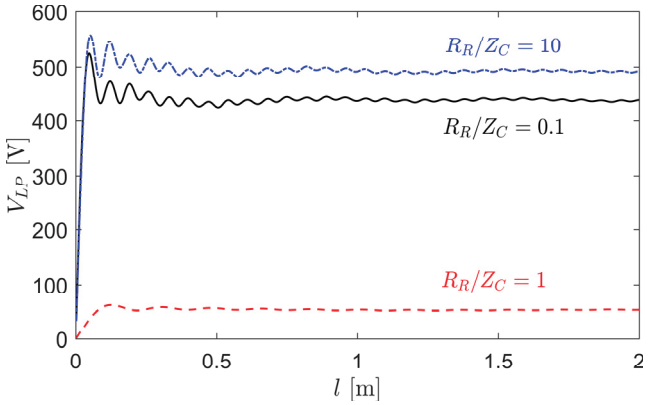

Fig. 7. Peak voltage V_{LP} vs harness length l for different R_R. Data: l =1 m, r_w=1 mm, h=1 cm, R_L=180 Ω, θ=60°, ϕ=120°, η=135°.

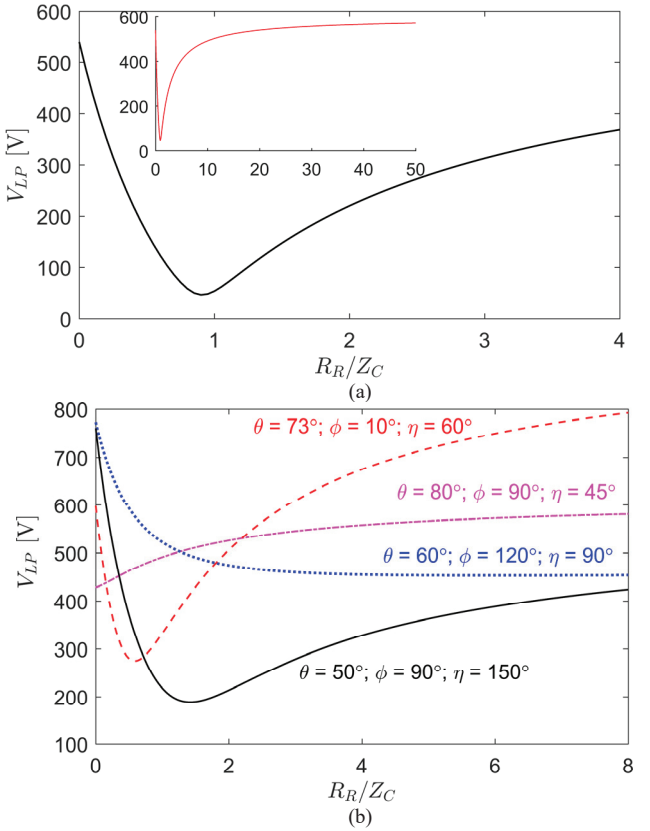

Fig. 8. Peak voltage V_{LP} vs R_R/Z_C for (a) θ=60°, ϕ=120°, η=135°; (b) other specified wave angles. Data: l =1 m, r_w=1 mm, h=1 cm, R_L=180 Ω.

of generality, the following simulation refers to data in Section II.C, unless differently specified. General properties can be inferred from the interpretation of the obtained results.

First, the worst-case voltage peak is plotted versus l and for different values of R_R/Z_C in Fig. 7, where one can note that V_{LP} still *converges to a stable value for long lines* (mismatching increases the frequency of oscillations). Though a closed-form expression of the asymptote is not available for mismatched R_R, the condition (15) for matched lines remains suitable to discriminate, at large, between a long and a short line.

By comparing Fig. 6 and Fig. 7, one could observe that V_{LP} is much greater for an unmatched load at the opposite line

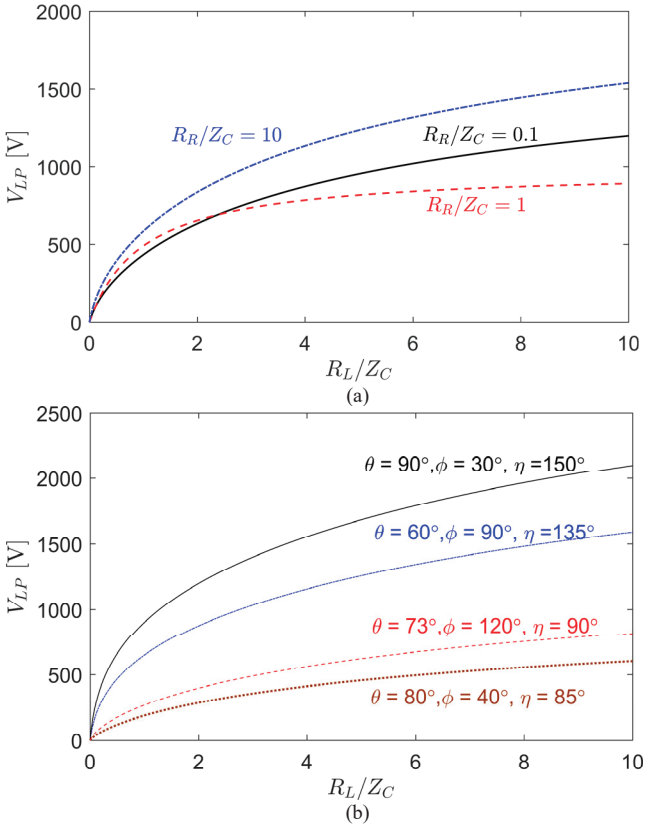

Fig. 9. Peak voltage V_{LP} vs R_L/Z_C for (a) different R_R with θ=60°, ϕ=120°, η=135°; (b) R_R=10 Ω with specified wave angles. Other data: l =1 m, r_w=1 mm, h=1 cm.

terminal than for a matched one. This aspect is better investigated in Fig. 8(a), where the worst-case voltage peak is plotted versus the normalized load coefficient R_R/Z_C spanning from 0 to 4 (a broader range 0-50 is presented in the inset). In general, the minimum of V_{LP} does not necessarily occur in case of perfect matching (i.e., for R_R/Z_C=1), as put into evidence in Fig. 8(b) where different wave angles are considered. Furthermore, for some combinations of angles, the curves in Fig. 8(b) are simply monotonic.

The impact of the resistive load R_L connected at the port of interest is much simpler, as highlighted by Fig. 9, where the worst-case voltage peak is plotted versus the normalized load R_L/Z_C for different opposite loads [Fig. 9(a)] and for different wave angles [Fig. 9(b)]. All the curves are monotonically increasing with R_L and, in the special case of matched opposite load (R_R/Z_C=1), V_{LP} converges to the value $V_\infty = 4h|G|\sqrt{Z_0 WB}$ for $R_L \to \infty$ according to (16).

The voltage peak is plotted versus the pulse bandwidth B in Fig. 10. In this simulation, the lower frequency f_1=300 MHz is kept fixed, while the upper frequency f_2 is increased from 300 MHz to 3 GHz, therefore B spans from 0 to 2.7 GHz. One can observe that the worst-case voltage peak is a *monotonically increasing function of the pulse bandwidth*, conforming to the general concept that, for the same signal energy, a narrowband pulse has less disrupting potential with respect to a broadband pulse containing that narrowband [1].

Finally, Fig. 11 shows the voltage peak versus line height for $h>4r_w$. Since the characteristic impedance Z_C changes with h,

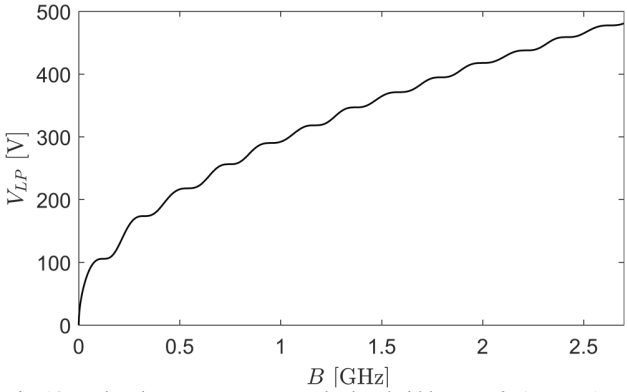

Fig. 10. Peak voltage V_{LP} vs HPEM pulse bandwidth. Data: l =1 m, r_w=1 mm, h=1 cm, R_L=180 Ω. R_R=10 Ω, θ=60°, ϕ=120°, η=135°.

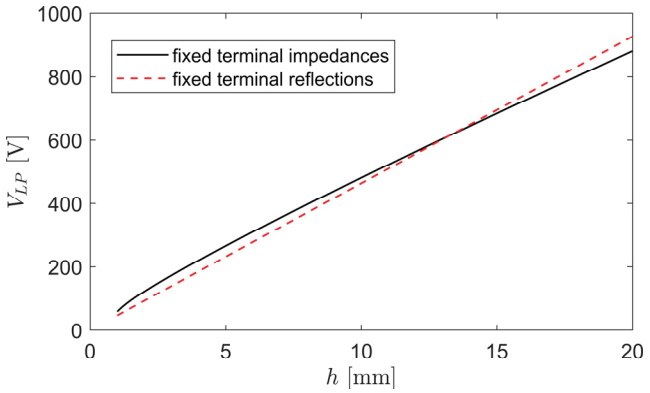

Fig. 11. Peak voltage V_{LP} vs line height h, for fixed resistances R_L =180 Ω, R_R=10 Ω, or fixed ratios R_L/Z_C=1, R_R/Z_C=0.1. Other data: l =1 m, r_w=1 mm, h=1 cm, θ=60°, ϕ=120°, η=135°.

two curves are plotted: (a) for fixed load resistances, and (b) for variable resistances such that the ratios R_L/Z_C, R_R/Z_C are constant. The increase of voltage with line height results to be *almost proportional* and, specifically, true linearity is obtained by keeping constant the loads' mismatching.

IV. Statistics of the Worst-Case Voltage Peak

In any realistic radiated-IEMI scenario, the direction of incidence and the polarization of the electromagnetic field are fully unknown and potentially distributed in their whole definition range [12], [13]. Since the response of the victim harness strongly depends on these quantities, the proposed analysis can take advantage from a statistical description of angles θ, ϕ, η as RVs, for a probabilistic assessment of IEMI effects. In particular, the full lack of knowledge can be adequately accounted for by assigning three independent and uniformly (U) distributed RVs

$$\theta \sim \mathrm{U}[0°, 90°]; \phi \sim \mathrm{U}[0°, 360°]; \eta \sim \mathrm{U}[0°, 360°] \quad (17)$$

Consequently, the worst-case CM voltage peak turns out to be a RV as well, which can be completely characterized by its empirical cumulative distribution function (cdf) evaluated through repeated-run simulations. To this aim, the proposed TL model is much more efficient than the reciprocity-based approach presented in [1], since the variation of geometrical and electrical parameters can be managed without performing time-consuming re-evaluations of the radiation pattern through full-wave solvers. The cdf of the worst-case voltage peak is exemplified here with reference to the data in Section II.C (unless differently specified) and is obtained by processing 10^5 Monte Carlo simulations, each one corresponding to a different illuminating condition, that is, a triplet of RVs generated according to (17). The voltage peak V_{LP} will range from zero (for specific angles which do not lead to field-coupling effects) to extreme values on the order of several hundreds of Volts. Such a large variability justifies the need for a statistical description.

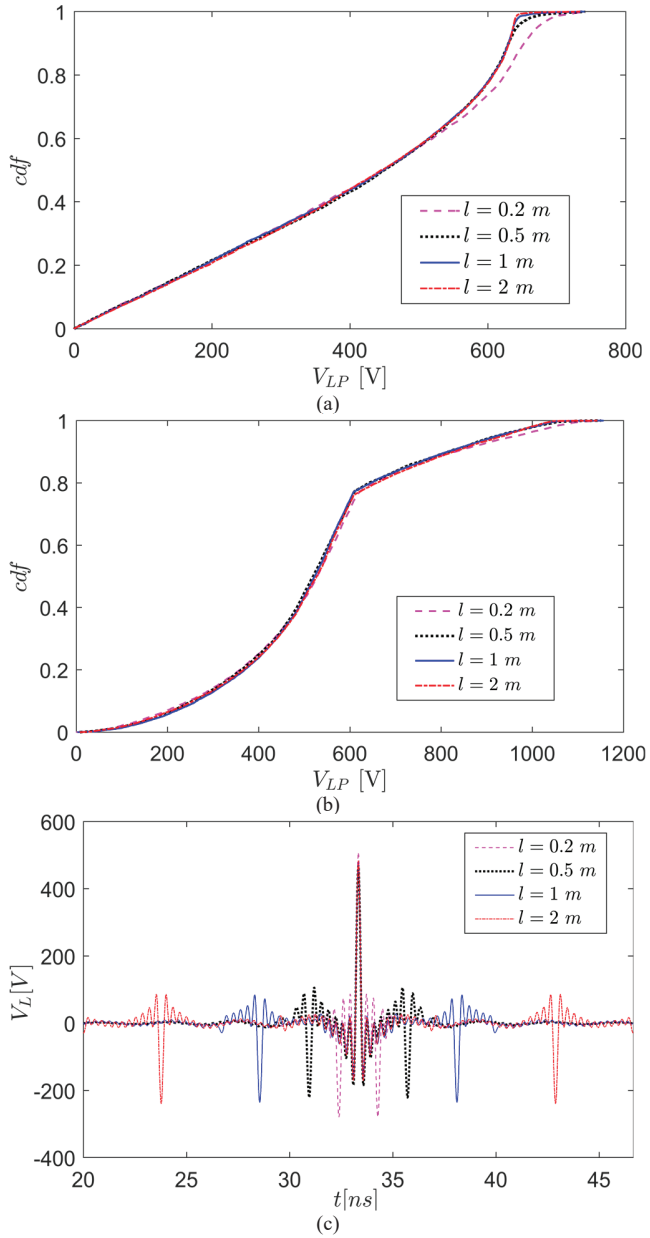

Fig. 12. Cdf of the worst-case voltage peak V_{LP} for different wire lengths l specified in the legend, r_w=1 mm, h=1 cm, in two loading cases: (a) R_R = 180 Ω (matched load); (b) R_R = 10 Ω. Waveforms of the induced voltage are shown in (c) for R_R = 10 Ω, θ=60°, ϕ=120°, η=135°.

To investigate the role of the harness length, the cdf of the worst-case CM voltage peak is plotted in Fig. 12 for different values of l (specified in the legend) and for two different terminal resistors connected to the far-end port: R_R=Z_C=180

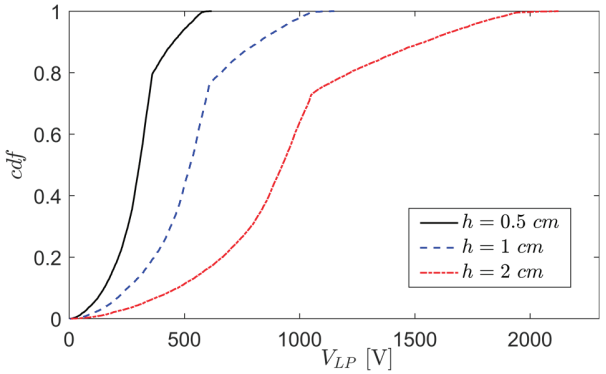

Fig. 13. Cdf of the worst-case voltage peak V_{LP} for different wire heights h, specified in the legend. Data: l =1 m, r_w=1 mm, R_L=180 Ω. R_R=10 Ω.

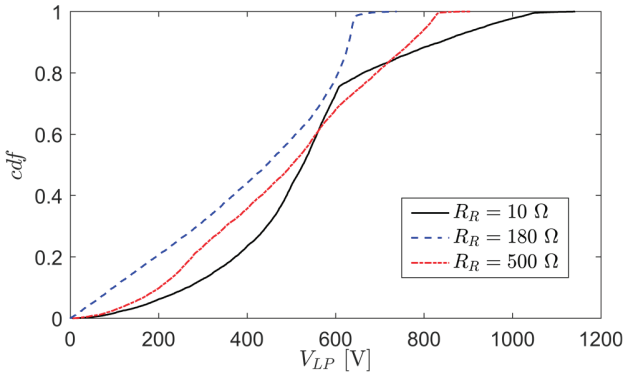

Fig. 14. Cdf of the worst-case voltage peak V_{LP} for different terminal resistors R_R specified in the legend. Data: l =1 m, r_w=1 mm, h=1 cm, R_L=180 Ω.

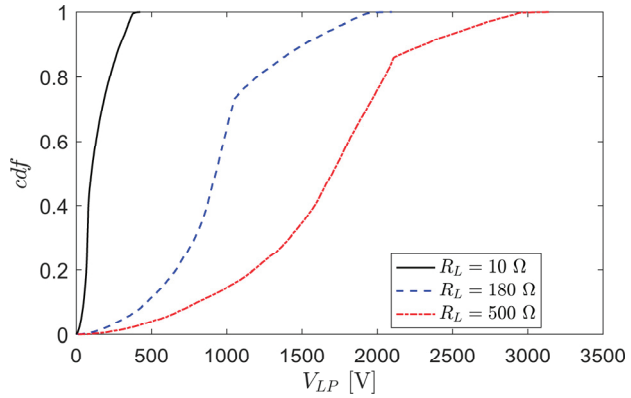

Fig. 15. Cdf of the worst-case voltage peak V_{LP} for different terminal resistors R_L specified in the legend. Data: l =1 m, r_w=1 mm, h=1 cm, R_R=10 Ω.

Ω [matched load, see Fig.12(a)], and R_R=10 Ω [see Fig.12(b)]. In line with the properties discussed in Section III, one can observe that the cdf is practically not affected by the harness length, both in case of a matched and an unmatched TL at the opposite line end. Minor variations can be appreciated just for the shortest length l=0.2 m, because it does not satisfy the condition (15) for *a few* of the possible incidence directions. It is therefore confirmed that *for long harnesses*, *the statistics of the worst-case voltage peak is not affected by the actual line length*.

In this connection, Fig. 12(c) instructively shows the waveforms of the worst-case induced voltage for a specific angle triplet (θ=60°, ϕ=120°, η=135°), R_R=10 Ω and four

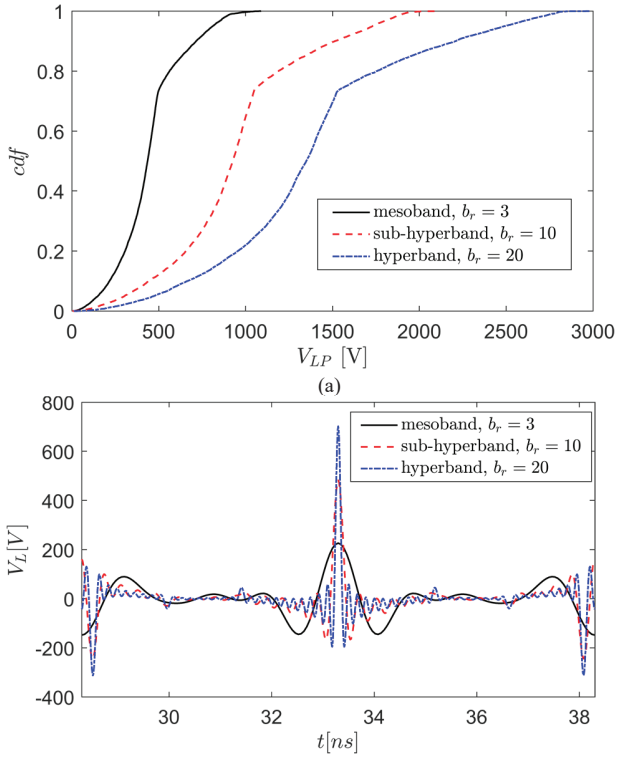

Fig. 16. (a) Cdf of the worst-case voltage peak V_{LP} for different wideband HPEM pulses, with band-ratio specified in the legend. (b) Waveforms of the induced voltage V_L are exemplified for θ=60°, ϕ=120°, η=135°. Data: l =1 m, r_w=1 mm, h=1 cm, R_L=180 Ω, R_R=10 Ω.

different lengths. In the plotted curves, the main peak (occurring at t_0=33 ns) remains the same, whereas the waveform is stretched for increasing line lengths, according to the increased time delay of travelling waves along the TL.

Concerning the impact of the line height, three cdfs of V_{LP} are presented in Fig. 13 for h=0.5 cm, 1 cm, 2 cm. As a confirmation to Section III, *the quantiles of the cdf result to be almost linearly rescaled* with the line height. For instance, the extreme values (quantile 1) of V_{LP} result to be 618 V, 1151 V, and 2124 V, respectively.

The complex effect of the opposite resistor R_R on the distribution of V_{LP} can be appreciated in Fig. 14, where the cdf of the worst-case voltage peak is plotted for three values R_R = 10 Ω, 180 Ω, 500 Ω, chosen to represent different loading conditions (i.e., less, equal and greater than the characteristic impedance, respectively). It results that the shape of the cdf is strongly modified by R_R in a nontrivial fashion. Nevertheless, a general property can be inferred, which was not self-evident in Section III. Namely, Fig. 14 clearly shows that the cdfs corresponding to the unmatched opposite loads lie entirely on the right of the one associated with a matched load. Hence, although it was observed [see Fig. 8(b)] that unmatched R_R can both increase or decrease the worst-case voltage peak for specific wave angles, by looking at the cdf (which globally encompasses all possible angles in a probabilistic description) one can conclude that *all the quantiles are increased by unmatched loads connected to the opposite line end.*

About the impact of load R_L at the port of interest, three cdfs of V_{LP} are shown in Fig. 15 for R_L = 10 Ω, 180 Ω, 500 Ω. In this case, the plot confirms the *monotone increase of the worst-case*

voltage peak for increasing resistances (predicted in Section III) while the cdf is globally subject to a nontrivial change of shape.

Finally, the statistical analysis is applied in Fig. 16(a) to investigate the impact of the HPEM pulse bandwidth. Once the bandratio is defined as $b_r=f_2/f_1$, wideband HPEM pulses can be classified as hypoband for $b_r\leq1.01$, mesoband for $1.01\leq b_r\leq3$, sub-hyperband for $3\leq b_r\leq10$, and hyperband for $10\leq b_r$, [2]. With these definitions, three bandwidths are considered. The lower frequency limit is fixed to f_1=300 MHz, whereas the upper frequency falls into different categories, namely, mesoband with b_r=3 (f_2=900 MHz), sub-hyperband with b_r=10 (f_2=3 GHz) and hyperband with b_r=20 (f_2=6 GHz). As in previous cases, all pulses have equal energy density 1 mJ/m^2.

The cdfs in Fig. 16(a) show *the uniform increase of quantiles for wider bandwidths*, with a general preservation of the distribution shape, which confirms the disrupting potential associated with wideband IEMI. For a specific triplet of angles (i.e., θ=60°, ϕ=120°, η=135°) the worst-case induced-voltage waveform is exemplified in Fig. 16(b), where one can appreciate the faster signals and the increasing peak, passing from the mesoband to the hyperband case.

V. Conclusions

In this paper, TL theory has been used to predict worst-case effects of the coupling of a radiated, wideband electromagnetic field to a cable harness above ground. The dominant CM coupling mechanism has been investigated, and precise conditions have been found, under which an HPEM pulsed field, with given bandwidth and finite energy density, leads to the maximum value of the induced CM voltage peak V_{LP} across a loaded cable terminal. This value is referred to as *worst-case* voltage peak and represents a summarizing figure of merit of the whole voltage waveform, for characterizing the complex IEMI phenomenon and to predict the potential susceptibility of the system in the most unfavorable conditions, depending only on its field-coupling properties.

Depending on the direction of incidence and the polarization of the electromagnetic field, the worst-case voltage peak is variable from zero (for specific illuminating conditions unable to couple the cable harness) to values spanning several orders of magnitude. It is therefore necessary to adopt a statistical description and compute the empirical cdf of V_{LP} through Monte Carlo repeated-run simulations. To this aim, the computationally efficient TL model here proposed is best suited to the analysis of cable harnesses, compared to the full-wave approach presented in [1].

Analytical derivations and numerical simulations have been presented to investigate the impact of system parameters on the statistics of the worst-case voltage peak. In particular, closed-form expressions have been derived in the special case of a matched load connected to the opposite line end. For other loading conditions, several simulations have been carried out to infer general properties. The main conclusions drawn from the study can be summarized as follows.

1) The condition derived in (15) defines a sort of critical length which can be used to discriminate between short and long harnesses. While for a short harness V_{LP} increases almost linearly with the cable length, for a long harness V_{LP} and its statistics do not depend on such a parameter.
2) For increasing line heights h, the increase of V_{LP} and its quantiles are approximately proportional.
3) The load R_R connected to the opposite line end plays a complex role (discussed in Sec. III). Nevertheless, as far as the cdf of V_{LP} is concerned, one can observe a general increase of quantiles for increased mismatching (both in case of less and greater resistances compared to the characteristic impedance). The effect of the load R_L at the port of interest is simpler, as V_{LP} and its quantiles exhibit a monotonic increase with this resistance.
4) The worst-case voltage peak V_{LP} and its quantiles are monotonically increasing with the HPEM pulse bandwidth.

These results offer insight into possible detrimental effects in terms of peak value of the CM voltage waveform, once associated with information about the immunity of terminal interfaces (common-mode rejection, susceptibility threshold). In this connection, one should recognize that the failure mechanism of equipment could be correlated also to other norms (e.g., peak derivative, energy, etc.) of the induced signal [14]. This seems suggesting that different optimization problems (like the one in Section II) could be considered and compared, for a future extension of the proposed rationale.

References

[1] G. Spadacini, T. Liang, F. Grassi, and S. A. Pignari, "Worst case and statistics of waveforms involved in wideband intentional electromagnetic attacks," *IEEE Trans. Electromagn. Compat.*, vol. 60, no. 5, pp. 1436-1444, Oct. 2018.

[2] D. V. Giri and F.M. Tesche, "Classification of intentional electromagnetic environments (IEME)," *IEEE Trans. Electromagn. Compat.,* vol. 46, no. 3, pp. 322-328, 2004.

[3] D. Månnson, R. Thottappillil, T. Nilsoon, O. Lundén, M. Bäckström, "Susceptibility of civilian GPS receivers to electromagnetic radiation," *IEEE Trans. Electromagn. Compat.,* vol. 50, no. 2, pp. 434-437, May 2008.

[4] F. Brauer, F. Sabath, and J. L. ter Haseborg, "Susceptibility of IT network systems to interferences by HPEM," in *Proc. 2009 IEEE Int. Symp. on Electromagn. Compat.*, Austin, TX, Aug. 17-21, 2009, pp. 237-242.

[5] F. Brauer, F. Sabath, and J. L. ter Haseborg, "Investigation of hardening measures for IT equipment against radiated and conducted IEMI," *IEEE Trans. Electromagn. Compat.,* vol. 54, no. 5, pp. 1055-1065, Oct. 2012.

[6] N. Mora, I.D. Flintoft, L. Dawson, J. F. Dawson, F. Rachidi, M. Rubinstein, A. Marvin, P. Bertholet, and M. Nyffeler, "Experimental characterization of the response of an electrical and communication raceway to IEMI," *IEEE Trans. Electromagn. Compat.,* vol. 58, no. 2, pp. 494-505, 2016.

[7] B. van Leersum, J. van der Ven, H. Bergsma, F. Buesink, and F. Leferink, "Protection against common mode currents on cables exposed to HIRF or NEMP," *IEEE Trans. Electromagn. Compat.,* vol. 58, no. 4, pp. 1297-1305, Aug. 2016.

[8] C. R. Paul, *Analysis of Multiconductor Transmission Lines*. New York: John Wiley & Sons, 2008.

[9] F. Rachidi, "A review of field-to-transmission line coupling models with special emphasis to lightning-induced voltages on overhead lines." *IEEE Trans. Electromagn. Compat.* vol. 54, no. 4, pp. 898-911, 2012.

[10] CST Microwave Studio, User Manuals, Dassault Systemes, VelizyVillacoublay, France, 2018. [Online]. Available: http://www.cst.com

[11] T. Liang, G. Spadacini, F. Grassi, and S. A. Pignari, "Coupling of wideband radiated IEMI to wiring harness: a statistical analysis of the main influencing parameters," in *Proc. 2018 IEEE Symp. on Electromagn. Compat.*, Long Beach, CA, USA, Aug. 2018.

[12] D. Nitsch, M. Camp, F. Sabath, J. L. t. Haseborg, and H. Garbe, "Susceptibility of some electronic equipment to HPEM threats," *IEEE Trans. Electromagn. Compat.,* vol. 46, pp. 380-389, 2004.
[13] W. A. Radasky, "The threat of intentional interference (IEMI) to wired and wireless systems." in *Proc. EMC-Zurich 2006 Int. Symp. on EMC,* pp. 160-163, 2006.
[14] D. V. Giri, High-power electromagnetic radiators: nonlethal weapons and other applications. Cambridge, MA: Harvard University Press, 2004.

Tao Liang received the B.Sc. and M.Sc. degrees in electrical engineering from Xi'an Jiaotong University, Shaanxi, China, in 2013 and 2016 respectively. He is currently working towards the Ph.D. degree in electrical engineering at Politecnico di Milano, Italy. His research focuses on electromagnetic compatibility modeling and testing techniques.

Giordano Spadacini (M'07–SM'16) received the Laurea (M.Sc.) and Ph.D. degrees in electrical engineering in 2001 and 2005, respectively, from Politecnico di Milano, Italy, where he is currently an Associate Professor with the Dept. of Electronics, Information and Bioengineering. His research interests include statistical models for the characterization of interference effects, distributed parameter circuit modeling, experimental procedures and setups for EMC testing, and EMC in aerospace and railway systems.
Dr. Spadacini has been Distinguished Reviewer of the IEEE EMC Transactions from 2014 to 2017. He is a recipient of the 2005 EMC Transactions Prize Paper Award, the 2016 Richard B. Schulz Best Transactions Paper Award, two Best Symposium Paper Awards from the 2015 Asia-Pacific Int. Symp. on EMC (APEMC) and the 2018 Joint IEEE EMC & APEMC Symposium.

Flavia Grassi (M'07–SM'13) received the Laurea (M.Sc.) and Ph.D. degrees in electrical engineering from Politecnico di Milano, Italy, in 2002 and 2006, respectively, where she is currently an Associate Professor with the Dept. of Electronics, Information and Bioengineering. From 2008 to 2009, she was with the European Space Agency (ESA), The Netherlands, as a Research Fellow. Her research interests include distributed parameter circuit modeling, statistical techniques, characterization of measurement setups for EMC testing, and powerline communications.
Dr. Grassi was awarded the URSI Young Scientist Award in 2008, and the IEEE Young Scientist Award at the 2016 Asia-Pacific Int. Symp. on EMC (APEMC). She was a recipient of the IEEE EMC Society 2016 Transactions Prize Paper Award, and of the Best Symposium Paper Award from the 2015 APEMC and from the 2018 Joint IEEE EMC & APEMC Symposium.

Sergio Amedeo Pignari (M'01–SM'07–F'12) received the Laurea (M.Sc.) and Ph.D. degrees in electronic engineering from Politecnico di Torino, Italy, in 1988 and 1993, respectively.
From 1991 to 1998, he was an Assistant Professor with the Dept. of Electronics, Politecnico di Torino, Turin, Italy. In 1998, he joined Politecnico di Milano, Milan, Italy, where he is currently a Full Professor with the Dept. of Electronics, Information, and Bioengineering, and Chair of the B.Sc. and M.Sc. Study Programs in Electrical Engineering. His research interests are in the field of EMC and include field-to-wire coupling and crosstalk, conducted immunity and emissions in multi-wire structures, statistical techniques for EMC, and experimental procedures and setups for EMC testing. His research activity is mainly related to Aerospace, Automotive, Energy, and Railway industry sectors.
Dr. Pignari is a recipient of the 2005 and 2016 IEEE EMC Society Transactions Prize Paper Award, and a 2011 IEEE EMC Society Technical Achievement Award. He is currently serving as an Associate Editor of the IEEE Transactions on EMC. From 2010 to 2015 he served as the IEEE EMC Society Chapter Coordinator. He has been Technical Program Chair of the ESA Workshop on Aerospace EMC in 2009, 2012, and 2016, and a Member of the Technical Program Committee of the Asia Pacific EMC Week since 2010.